An Experimental Approach for Correlation of the Magnetic Barkhausen Noise to Microstructural Changes and Residual Stress in Welding Joints

Olga Liskevych[1] (iD), Ana Paula Favero Fiorin[1] (iD), Elton Mesquita de Almeida[2] (iD), Gabriel Fracalossi Feijó[2,3] (iD), Rogério Lima Mota de Oliveira[4] (iD), Marcelo Camargo Severo de Macêdo[1,3] (iD)

[1] Universidade Federal do Espírito Santo – UFES, Departamento de Engenharia Mecânica, Vitória, ES, Brasil.
[2] Centro de Pesquisa, Inovação e Desenvolvimento – CPID, Laboratório de Ensaios Não-Destrutivos – LABENDEM, Cariacica, ES, Brasil.
[3] Universidade Federal do Espírito Santo – UFES, Programa de Pós-graduação em Engenharia Mecânica – PPGEM, Vitória, ES, Brasil.
[4] Instituto Federal de Santa Catarina – IFSC, Engenharia Mecânica, Xanxerê, SC, Brasil.

Abstract: Accurate measurement of the residual stress in welded joints is still a major challenge for both welding quality control and non-destructive testing. One of the most recent and innovative magnetic techniques for this purpose, known as Magnetic Barkhausen Noise (MBN), is based on the reorganization of magnetic domains (regions with uniform magnetic orientations) in the presence of a varying magnetic field in the studied ferromagnetic material. A significant difficulty in using this method for the analysis of welded joints lies in evaluating of the contribution that each altered material property induces in the resulting noise signal. Therefore, the objective of this study was to correlate the MBN signal with the typical changes that occur in the weld bead and its specific regions during the welding process applied to ASTM A36 steel. Thus, the root mean square (RMS) value of the signal was correlated with micro- and macrostructural changes in the joint, as well as with hardness and residual stress state, including its tensile and compressive magnitudes, demonstrating to be an effective non-destructive tool for characterizing of welded structures.

Key-words: Magnetic Barkhausen Noise; Welding; Residual stress; Hardness; Microstructure.

1. Introduction

Welding procedure is commonly used to join metal components in various industries; however, it introduces two significant challenges: thermal and residual stresses. During the welding process, intense heat is applied, causing local expansion and contraction in the welded region. As the joint cools down, differential thermal stresses develop, potentially leading to distortion, cracking, or even failure of the welded structure. Moreover, after welding, the residual stress remains locked within the material due to non-uniform cooling and phase transformations [1].

Accurate measurement of residual stress in welded joints is still a major challenge for both welding quality control and non-destructive testing. On the one hand, although its influence has been reported many times for relevant consequences of material processing, such as dimensional stability and distortions [2-7], fatigue life [8-11] and hot cracking occurrence [12], the main standards in welding engineering [13,14] do not determine residual stress evaluation as mandatory for the qualification and implementation of welding procedures. On the other hand, residual stress estimation relies on a variety of numerical, experimental non-destructive and semi-destructive methods, each with its own performance, cost, complexity, precision and accuracy of the obtained results, which can frequently make difficult an objective and comparable analysis of the welding impact on the stress changes in mechanical components.

Guo et al. [15] in their detailed review of recent advances in residual stress evaluation methods distinguish techniques indicated to surface and internal measurements. The first group is mainly represented by the nanoindentation technique, ring-core and hole-drilling methods, whereas the second one is based on diffraction, ultrasonic and magnetic phenomena. Among these methods, magnetic techniques stand out due to their capability to assess the internal material layers, as well as their rapidity and practicality. The basic principle of these techniques is based on changes of the ferromagnetic material properties when magnetized. For example, when a material is under stress, its permeability changes accordingly. The relative change in magnetic permeability is proportional to the stress, and the residual stress can be determined by measuring the change in total magnetic resistance in the magnetic circuit [16].

One of the most recent and innovative magnetic techniques for residual stress evaluation, the Magnetic Barkhausen Noise (MBN) [17], is well known for its sensitivity to induced stresses [18-21], capability that has been shown so far to obtain information from different measurement depths [18-23] and portability of its measurement systems when compared to

An Experimental Approach for Correlation of the Magnetic Barkhausen Noise to
Microstructural Changes and Residual Stress in Welding Joints

Liskevytch et al.

conventional nondestructive residual stress depth-profile measurement systems, such as neutron and X-ray diffraction (XRD). Moreover, the test samples do not require any special pretreatment.

The principle of this method can be described in terms of the reorganization of magnetic domains (regions with uniform magnetic orientations) in the presence of a varying magnetic field in the studied ferromagnetic material. Under these conditions, forced reorganization tends to form larger domains oriented in specific directions, leading to abrupt movements that are influenced by micro and macrostructural factors of the material. These movements generate magnetic pulses (so-called magnetic noise) that can be measured as a sequence of voltage signals through a sensing coil placed on the investigated material surface, as shown in Figure 1. When the external magnetic field is parallel to the stress present in the material, the Barkhausen signal is proportional to the tensile stress and inversely proportional to the compressive stress [18-25].
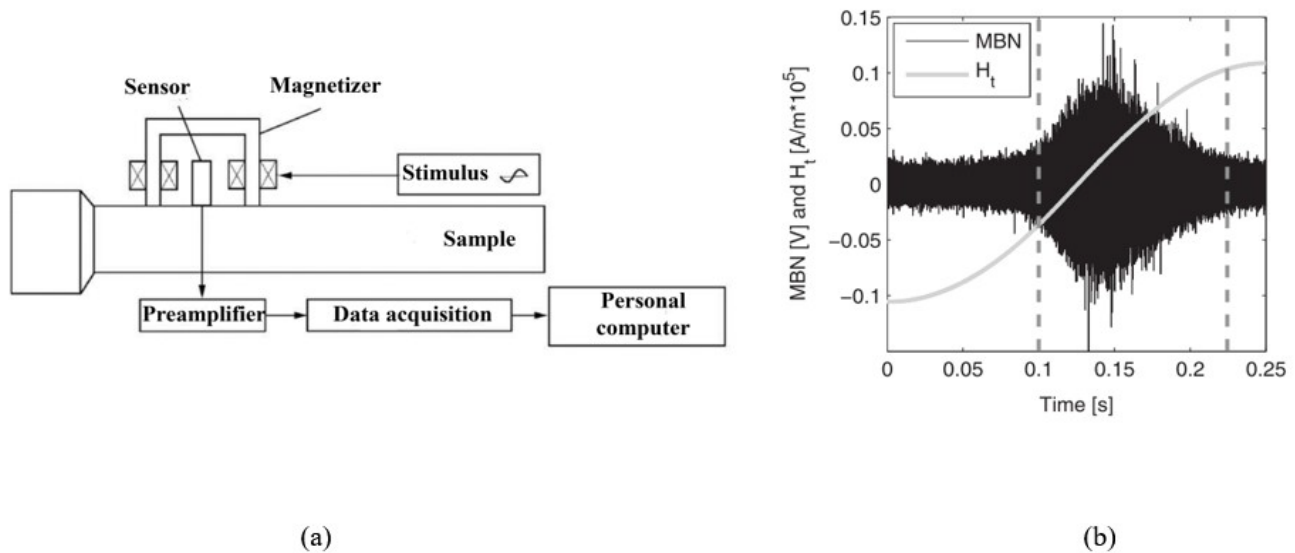

Figure 1. Magnetic Barkhausen Noise method basics: (a) MBN detection system [15] and (b) MBN and tangential magnetic field (H_t) signals and the peak region (between discontinuous vertical lines) which is used to calculate the MBN magnitude spectrum [24].

Despite its apparent simplicity, the use of this method for welded joints is not straightforward. The reason for this is owing to the sensitivity of the MBN parameters, in addition to residual stresses, also to microstructural changes, grain size, and microhardness [18,23,25,26]. As stated by Sorsa [27], this sensitivity arises from the influence of the material's microstructure on the magnetic domain structure and the distribution of anchor points. The locations of anchor points that alter the movement of the magnetic domain wall, affecting MBN, can include precipitates, grain boundaries, inclusions, dislocations, phase changes, among other factors.

As the welding procedure influences both the residual stress and the aforementioned characteristics, the results of using MBN in welds can sometimes be contradictory. Thus, when MBN was used to study the residual stress in electrical steel welded with the GTAW, PAW and EBW processes by Vourna et al. [23], the results demonstrated the coherence of the noise signal measured in various regions of the weld bead with the expected residual stress distribution (Figure 2a), even considering the typical HAZ width for each applied process. The signal exhibited higher values at the center of the weld bead (where, according to the theoretical models [1,29], the highest magnitude of the tensile residual stress is concentrated), intermediate values in the base metal region (where lower-magnitude compressive residual stress are concentrated), and alternated values in the HAZ (where the transition between tensile and compressive stresses occurs). Also, when compared to the stress values measured by XRD method, the MBN values showed a strong correlation.

In their turn, Serna-Giraldo and Padovese [28] also studied MBN application in welds (made of A36 structural steel using the SMAW process). However, the focus of this work was to relate the noise signal parameters to the final microstructure of the weld bead. The authors reported that the signal value decreased from the center of the weld bead to a point corresponding to the fusion line, as shown in Figure 2b. From this point, an increase in the signal was observed, and it stabilized at the point corresponding to the HAZ limit. This behavior of the MBN parameters was related by the authors to microhardness variations. They explained that at the fusion line, where an acicular microstructure with a higher density of dislocations is present, the highest hardness value and the lowest value of the MBN signal parameter were obtained. Dislocations act as barriers to domain wall movement, thus leading to low MBN emissions. Moving away from the fusion line, the cooling rate decreases, favoring a change in the acicular morphology of ferrite to a polygonal form, with the presence of coarser perlite colonies. A decrease in the grain size of both ferrite and perlite was also observed. These microstructures

An Experimental Approach for Correlation of the Magnetic Barkhausen Noise to
Microstructural Changes and Residual Stress in Welding Joints

Liskevytch et al.

exhibit lower hardness. As the grain refines, the number of moving domain walls increases, and the absence of an acicular structure causes the number of dislocations to decrease, reducing the barriers to domain movement and facilitating the movement of domain walls. This interaction results in higher MBN emission in HAZ. Both the cited studies used root mean square (RMS) values for the MBN analyses.
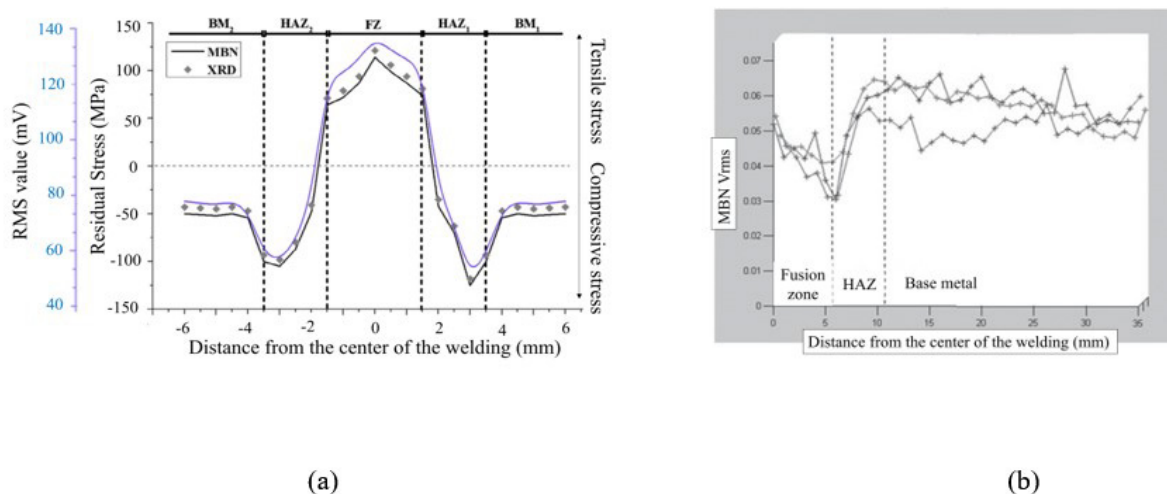

Figure 2. Different behavior of the MBN signal when applied to the welding joints: (a) associated to residual stress in GTAW welded electrical steel [23] and (b) associated to microhardness of SMAW welded structural steel [28].

Another conflicting point was raised by Yelbay et al. [25] in attempt to correlate MBN signal values with residual stress magnitudes in welded carbon steel plates. In this study, the specific stress versus MBN calibration set-up was used for the parent and HAZ material, and a strong data correlation for the BM was reported, while HAZ residual stress values exceeded the yield strength of the material at some points. The authors suggest that this incongruity may be resulted from using a single calibration curve for HAZ region, therefore, if practical, all zones having remarkably different microstructure should be separately considered in the calibration procedure. Otherwise, depending on the severity level of the microstructure effect on MBN emission, the residual stress values determined by MBN measurements may show deviations from the exact values.

Considering these challenges, the implementation of the MBN method in assessing welded joints requires careful attention and control over microstructural aspects to ensure precise and reliable outcomes. The presence of residual stresses and the influence of various microstructural elements necessitate a thorough consideration and analysis during the evaluation process. Therefore, the objective of this study was to correlate the MBN signal with the typical changes that occur in the weld bead and its specific regions after the welding process, and to deepen the application of this non-destructive test by performing a systematic analysis of the noise signal in a welding structure.

2. Methodology

2.1. Welding procedure

A welded sample with dimensions of 150mm × 120mm × 5mm was produced from ASTM A36 structural steel (the material properties are presented in Table 1) using the GMAW process, which employs an electric arc as the energy source for heating and fusion, and a shielding gas for welding pool protection. The welding parameters were kept constant at values of 27 V for voltage, 120 A for current (DC+), and 21.0 mm/s for welding speed. The single pass butt joint with an I-bevel was welded using a 1.0 mm diameter ER70S-6 electrode and a shielding gas composed of 75% Ar and 25% CO_2.

Table 1. Properties of ASTM A36 structural steel.

Property	Value
Density [g/cm^3]	7.8
Tensile strength [MPa]	400-550
Yield strength [MPa]	250
Elastic modulus [GPa]	200
Carbon content [%]	0.29

An Experimental Approach for Correlation of the Magnetic Barkhausen Noise to
Microstructural Changes and Residual Stress in Welding Joints

Liskevytch et al.

2.2. MBN measurement

To measure the MBN signal, an equipment constituted from Rollscan 350 Barkhausen Noise Analyser and S1-18-13-01 sensor with a 1 mm diameter was employed, according to illustrated in Figure 3a. This sensor model can be used for different surface finishing, guaranteeing a uniform contact that was prioritized in this study due to the characteristic convexity of the weld bead. To process the signal, MicroScan 600 software with a commercial algorithm was used, providing different output parameters. For the purposes of this work, only the RMS (Root Mean Square) values of the MBN signal were considered due to its confirmed sensitivity to microstructural changes and residual stress generation [23,28]. Moreover, Peak parameter results (another MBN parameter reported in the literature) did not provide any solid tendencies or conclusions during this study.

For the MBN measurement parameterization, the criterion of the highest magnetization amplitude of the sample was used, ensuring that the process remained unsaturated (which would make the measurement procedure unfeasible). To achieve this condition, the magnetization voltage and frequency were determined from the best stabilization index of the calibration curves, as shown in Figure 4. Thus, the setting test parameters are detailed in Table 2, including the measurement depth calculated according to the Equation 1 and the methodology proposed in Moorthy et al. [18].

$$\delta = \frac{1}{\sqrt{\pi f \sigma \mu_0 \mu_r}} \tag{1}$$

where f is the magnetization frequency, σ is the conductivity of the material, μ_0 is the permeability of vacuum and μ_r is the relative permeability of the material. For the ASTM A36 steel, the conductivity is 5.9×10^6 S/m, the low field μ_0 and μ_r were taken as 4×10^{-7} T×m/A and 200, respectively.
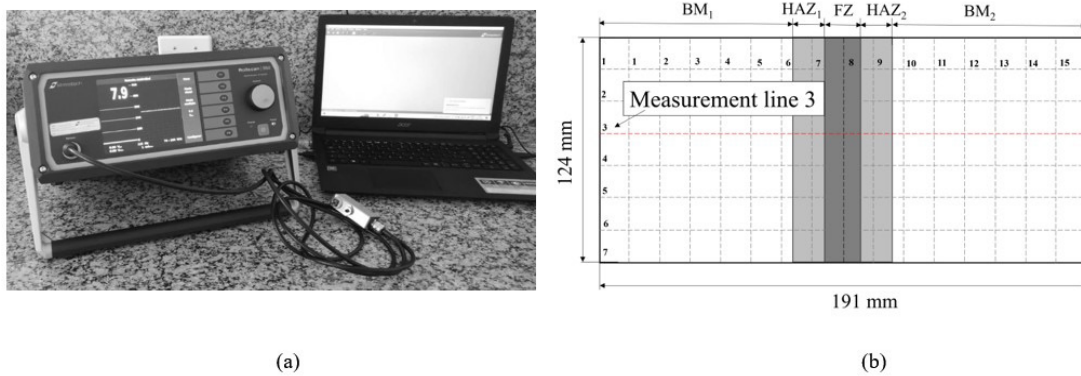
Figure 3. MBN signal measurements: (a) equipment arrangement and (b) measurement grid of the welded sample.
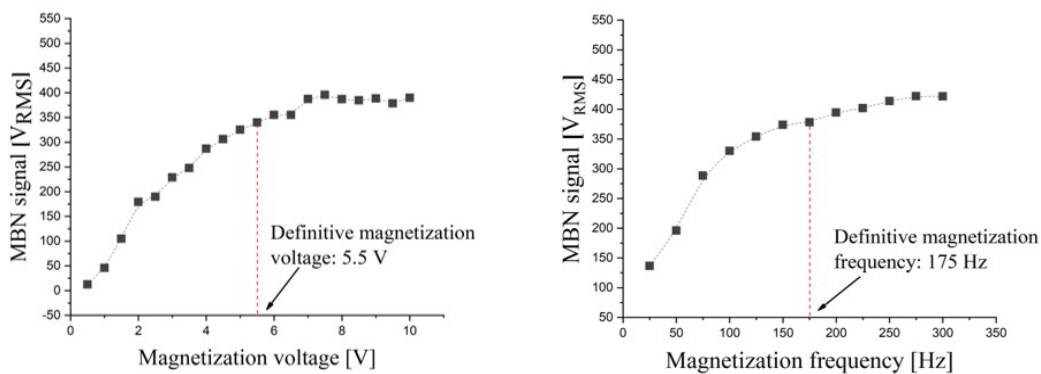
Figure 4. Calibration curves for the voltage and frequency of magnetization.

Table 2. Setting parameters of the MBN measurement test.

	Setting parameter	Value
Magnetic field properties	Magnetization voltage [V]	5.5
	Magnetization frequency [Hz]	175
Measurement characteristics	Acquisition frequency [MHz]	6.410
	Analyzed frequency range [kHz]	70-200
	Measurement depth [mm]	0.3

An Experimental Approach for Correlation of the Magnetic Barkhausen Noise to
Microstructural Changes and Residual Stress in Welding Joints

Liskevytch et al.

For definitive measurements of the RMS values of the MBN, the sample was demarcated, as shown in Figure 3b, ensuring complete scanning of the analyzed surface, including the base metal, fusion and heat-affected zones (BM, FZ and HAZ, correspondingly). Three repetitions were performed for each of the 105 squares with a 50 mm^2 area (compatible with the sensor probe area). During scanning, the position of the probe was carefully adjusted to ensure a full contact with the surface during the measurements. Subsequently, the matrix of the average RMS values was plotted on a heat map using interpolation functions. Additionally, the RMS values obtained along line 3 (Figure 3b) were correlated with the macrographic analyses, hardness values, and residual stress measured at the same location. It is worth mentioning that in order to avoid any influence of the material removal on the joint stress state, MBN measurements were taken prior to any other procedures.

2.3. Residual stress measurements

In order to compare the MBN signal with the residual stress distribution in the welded joint, the ESPI-based hole-drilling method was applied. The measurements were performed using the equipment shown in Figure 5a, which consists of a camera for image capture, drilling tool, sample fixture device, and laser beam with all its known properties. During the measurement procedure, the beam is divided into two parts: the first one is launched on the sample and reflected to the camera, whereas the second one (referred to as reference beam) passes through a piezoelectric phase change system and is subsequently directed to the same optical device. When a hole is drilled in the sample and the stress present in the material is relieved by local deformation, the light beam reflected from the surface of the sample changes its characteristics. When compared to the reference beam, the reflected beam exhibits a phase shift, which leads to a new grain pattern (pixels) in the recorded camera images. From the difference in pixel arrangement before and after drilling, that is, before and after stress relief, a speckle pattern is obtained (see Figure 5b). Subsequently, the spackle patterns are processed as digital interferograms [30] with an equipment algorithm in order to obtain the local surface displacements caused by the machining of the sample and the corresponding residual stress present in the material before drilling.

The aforementioned ESPI-based hole-drilling method has already been employed in residual stress studies [31-33], demonstrating an acceptable error of 3.5% for aluminum samples and 5% for steel samples. In this study, the equipment was previously calibrated using a standard four-point bending device [34], and a good accuracy also was reported (with a mean error of 5.8%), as well as a good precision (with a coefficient of variation of 6%) and excellent measurement sensitivity, even when applied to irregular surfaces of welded joints (more details in Liskevych et al. [35]).

Both for calibration purposes and definitive residual stress evaluation, series of measurements were carried out drilling 0.8 mm diameter hole at a rotational speed of 25000 rpm and 0.05 mm/s feed rate reaching the maximum hole depth of 0.4 mm. These parameters are recommended in the literature to achieve good-quality hole opening [31,36]. Furthermore, the employed diameter and depth of drilling were suitable to ensure the measurement of residual stress in the narrow regions of the fusion and heat-affected zones.

A reference stress was measured prior to welding, and afterwards, fallowing the MBN analyses, three measurements were taken in each studied region (FZ, HAZ and BM) using the referred ESPI-based hole-drilling method in order to investigate the impact of welding on the generation of tensile and compressive stresses in the joint. During machining, at each of 0.05 mm drilling increment, images were captured with interferometry pattern shifts due to the changes occurring in the stress state of the material. After interferograms processing, values of the measured stress in longitudinal direction (that is, longitudinal residual stress, parallel to the weld bead extension) in the depth of 0.3 mm (the same for MBN tests) were provided for the further analysis.
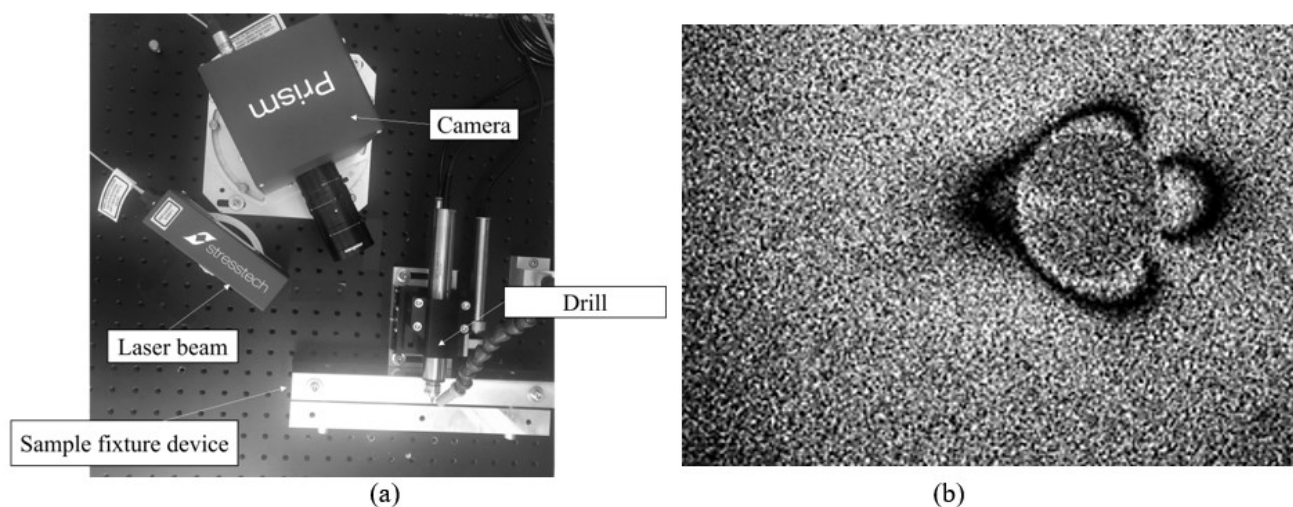

Figure 5. ESPI-based hole-drilling method employed for the residual stress measurements: (a) experimental arrangement; (b) speckles pattern caused by residual stress relief during the hole opening.

An Experimental Approach for Correlation of the Magnetic Barkhausen Noise to
Microstructural Changes and Residual Stress in Welding Joints

Liskevytch et al.

2.4. Macrography and hardness evaluation

From the resulting welded joint, a small rectangular specimen was carefully extracted in the transverse direction (approximately from measurement line 3, as illustrated in Figure 3b), in order to examine its microstructure, fusion and heat-affected zones dimensions, as well as the hardness changes due to the welding procedure. This specimen was cold mounded in resin, grounded using abrasive silicon carbide papers with nominal densities of 800, 1000, 1200 and 2000 and then polished with fine diamond paste. Finally, the polished sample was etched in a 2% Nital solution (2 ml HNO_3, 98 ml ethanol) for 20s at room temperature until the grain boundaries were revealed.

By employing a stereoscope and an optical microscope, it was possible to discern the dimensions of the fusion and heat-affected zones of the weld bead, as well as to analyze their microstructures. Hardness measurements were performed using a Vickers hardness tester operating at 200 nN and 0.5 mm increment. Indentations were carefully made on the polished sample's surface.

Both the FZ and HAZ dimensions, as well as hardness measurements were carried out at the 0.3 mm depth in order to relate these results with MBN analyses and residual stress values measured by the ESPI-based hole-drilling method.

3. Results

3.1. Macrography and hardness analysis

The cross-sectional profile of the resulting welded joint is shown in Figure 6. The width of the fusion zone (FZ) and heat-affected zone from both sides of the bead (HAZ_1 and HAZ_2) obtained from this profile at the depth of 0.3 mm are listed in Table 3. Considering these dimensions, it can be concluded that the 0.8 mm diameter hole in the residual stress measurement tests and the MBN sensor with a diameter of approximately 1 mm were suitable for characterizing these specific weld bead areas.

The microstructures of the different areas of the analyzed weld bead are shown in Figure 7. The BM area (where the maximum temperatures reached during the welding procedure were below the austenitization line, therefore, no phase transformation occurred) consists of ferrite and perlite phases with 11 – 15 μm average grain size. The FZ exhibits a typical solidification structure with grain orientations growing epitaxially towards the center of the weld bead. The microstructure consists of allotriomorphic ferrite at the grain boundaries with perlite plates. The HAZ area is narrow, and its microstructure is presented by primary ferrite at the grain boundaries. Distancing from the fusion line, the microstructure changes both in terms of grain size (which decreases) and morphology of ferrite, which becomes more polygonal. This occurs because of the lower maximum temperatures reached in this area preventing the growth of austenitic grains, and because of the slower cooling rates preventing the acicular microstructure formation.

Table 3. Width of the different weld bead regions at the depth of 0.3 mm [mm].

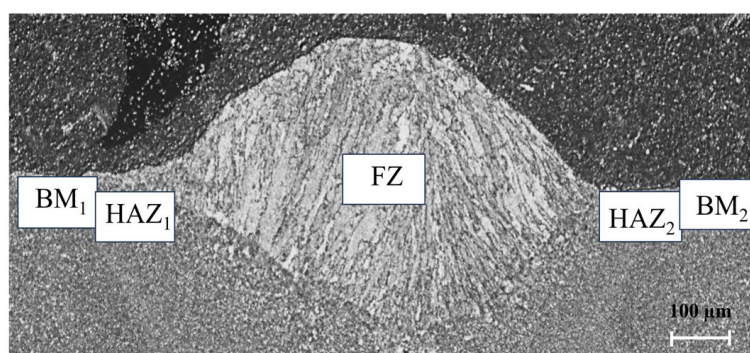| HAZ$_1$	FZ	HAZ$_2$
2.03	5.53	1.79

Figure 6. Cross-sectional area of the welded joint.

The hardness profile of the welded joint is shown in Figure 8. As can be observed, the FZ hardness exhibits the highest value with slight variation, probably, due to microstructural heterogeneities, as demonstrated in Figure 7a. At the fusion line, the hardness values decrease and then stabilize at their minimum values in the BM. Hardness typically increases in the FZ of the welded joint due to several factors associated with the welding process and metallurgical changes that occur during welding, among them, grain size and phase transformation. Rapid cooling of the molten metal in the FZ promotes the formation of smaller grain sizes in the microstructure and, in its turn, smaller grains tend to have higher hardness compared to larger grains because they limit the movement of dislocations within the crystal lattice. As for the phase transformations, a higher amount of perlite in the FZ can contribute to the hardness increase as well, since perlite is typically harder than ferrite phase also present in the FZ (Figure 7b).

An Experimental Approach for Correlation of the Magnetic Barkhausen Noise to
Microstructural Changes and Residual Stress in Welding Joints

Liskevytch et al.

Thus, the mean hardness was: 240 HV in the FZ, 184 HV and 189 HV in the HAZ_1 and HAZ_2, respectively, and 168 HV in both BM_1 and BM_2. Therefore, the welding procedure used in this study led to an increase in hardness of approximately 13% in the HAZ and 27% in the FZ.
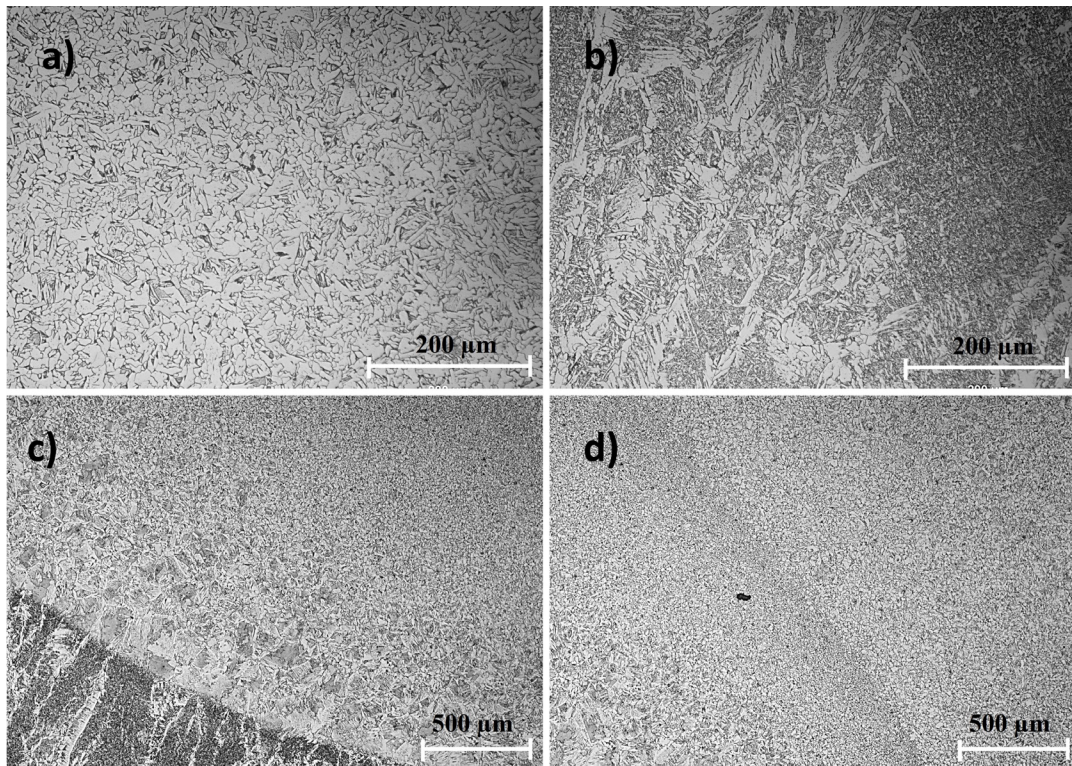

Figure 7. Microstructure of the welded joint: (a) BM, (b) FZ, (c) interface between HAZ and FZ, (d) transition regions from BM to FZ.
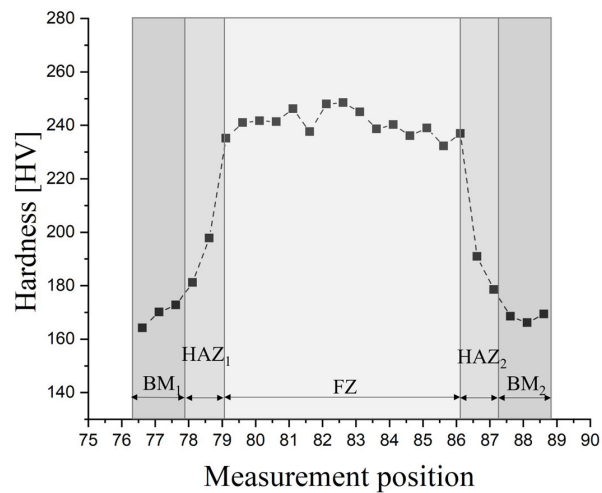

Figure 8. Hardness profile of the welded joint.

3.2. Residual stress analysis

The values of residual stress measured with the ESPI-based hole-drilling technique in different areas of the welded joint are presented in Table 4, and their distribution is illustrated in Figure 9. These stresses were found to be tensile in the FZ, also tensile but of lower magnitude in HAZ_1 and HAZ_2, and compressive (attributed to a balance between the molten and unaffected zone within the welded component) in BM_1 and BM_2 next to the fusion line, what is in accordance with existing theoretical models [1,29].

Due to the specificity of the applied measurement method, the stresses were obtained at different depths (0.2-0.35 mm), demonstrating a lower variation in the BM and HAZ, and a higher variation in the FZ. This result can be explained by the higher

An Experimental Approach for Correlation of the Magnetic Barkhausen Noise to
Microstructural Changes and Residual Stress in Welding Joints

Liskevytch et al.

heterogeneity in the chemical composition and microstructure of the melted and solidified material, which in turn leads to a higher variation in the properties of the FZ (for example, of the material yield strength) and a consequent higher variation of generated thermal stresses that depend on these properties. Thus, mean values of the residual stress present in the welded joint were reported as 198 MPa in the FZ (which is 79% of the material yield strength), 8.2 MPa and 10 MPa in the HAZ_1 and HAZ_2, and -96.1 MPa and -95.2 MPa in the BM_1 and BM_2, correspondingly.

For comparison purposes, Figure 10 presents the distribution of stresses at a measurement depth of 0.3 mm, which is the same depth where the RMS values of the MBN signal were obtained.

Table 4. Residual Stress [MPa] measured in different areas of the welded joint.

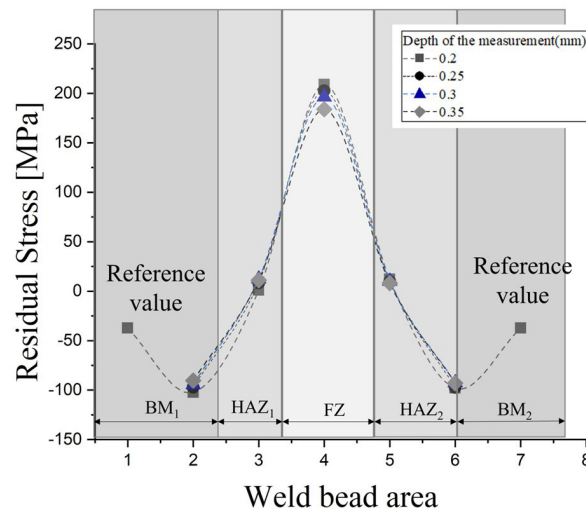| Measurement depth [mm]	BM_1	HAZ_1	FZ	HAZ_2	BM_2
0.2	-102.2	0.9	209.0	12.1	-98.0
0.25	-97.1	8.4	202.7	9.8	-97.4
0.3	-94.6	12.4	196.3	10.0	-92.5
0.35	-90.3	11.2	184.0	8.2	-93.0
Mean	-96.1	8.2	198.0	10.0	-95.2
SD	5.0	5.2	10.7	1.6	2.9

SD: Standard Deviation.

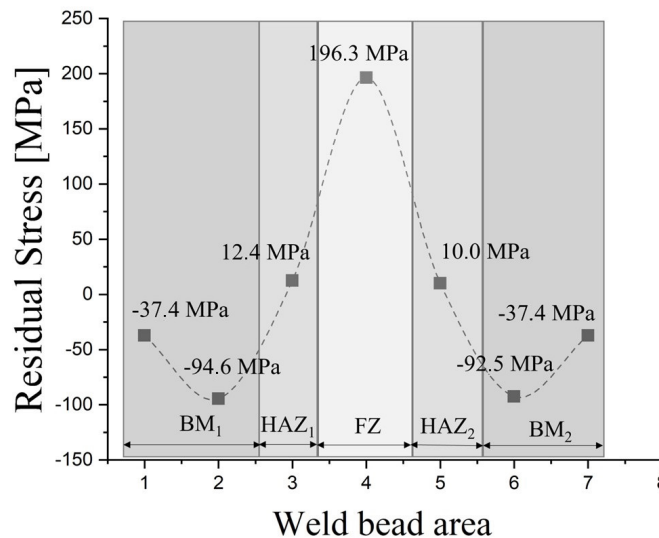**Figure 9.** Residual stress distribution in the welded joint at different measuremental depths.

Figure 10. Residual stress distribution in the welded joint at the depth of 0.3 mm.

An Experimental Approach for Correlation of the Magnetic Barkhausen Noise to
Microstructural Changes and Residual Stress in Welding Joints

Liskevytch et al.

3.3. MBN signal analyses

The result of the scanned MBN signal for the entire welded sample is presented in Figure 11 as a heat map of the RMS mean values measured according to illustrated in Figure 3b at the depth of 0.3 mm. It can be observed that, in general, the signal showed maximum values in the area corresponding to the weld bead, decreasing next to the FZ and displaying its minimum values in the area corresponding to the BM. Similar results for the distribution of the RMS values of the MBN in welded joints have been previously reported in Vourna et al. [23] and Serna-Giraldo and Padovese [28].

Figure 12 graphically represents the variation of the RMS values of the MBN measured along line 3 (as illustrated in Figure 3b) at the depth of 0.3 mm, where the sample was sectioned for macro and micrographic analysis and where the ESPI-based hole-drilling measurements of the residual stress were performed as well. For a repeatability purpose, the data obtained from lines 4 and 5 also were plotted, demonstrating good consistency of results. It can be observed that the highest signal magnitude was obtained at the location corresponding to the FZ, decreasing then to the location corresponding to the fusion line and the beginning of HAZ_1 and HAZ_2. From this point, a small increase in the signal is noticeable in both the thermally affected areas. Subsequently, the signal decreases until the transition line between the HAZ and BM, reaching its minimum value in the BM. Beyond this point, the MBN signal increases and stabilizes at the edges of the welded joint.

When relating the MBN signal reported in Figure 12 to the hardness results presented in Figure 8 and residual stress results presented in Figure 10, a strong correlation can be observed between the signal variation and the analyzed properties of the welded joint. Generally, the increase in the MBN values followed an increase in the hardness and tensile stresses in the FZ. However, while the results related to residual stress are consistent with previously published reports [23,30], where higher RMS values for greater tensile stress magnitudes were also observed, the increase in the MBN signal with increasing hardness in the FZ differs from the observations reported by Moorthy et al. [18], as shown in Figure 2b. As stated by the authors, in the FZ (where a microstructure with a higher density of dislocations and higher hardness value is present), the dislocations would act as barriers to the movement of the domain walls during magnetization, thus decreasing the MBN signal, which was not observed in the present study. This can be explained by the contribution of the hardness and residual stress to the MBN changes in the FZ. Thus, the welding procedure applied in this study increased the hardness value in this area by 27%, whereas the same welding procedure increased the residual stress values by approximately 119%, demonstrating that the residual stress influence on the measured RMS values of the signal was significantly higher than that of the microstructure changes.

Nevertheless, in this context, it is interesting to note that the increase in the MBN signal in HAZ_1 and HAZ_2 did not correlate with the gradual decrease in residual stress values at this location (see Figure 10). This signal behavior was likely caused by the change in the grain size in the HAZ, i.e., its growth apart from the fusion line and subsequent refinement (see Figure 11c). In the grain growth area, the number of moving domain walls during magnetization decreases, and the absence of an acicular structure reduces the number of dislocations, decreasing the barriers to domain movement, thus increasing the MBN signal during the test. As soon as the grain refines, the number of barriers increases, thereby decreasing the MBN signal. A similar tendency has been reported previously by Ktena et al. [30], leading to the conclusion that, unlike in the FZ, in the HAZ, the prevalent influence on the measured RMS values of the MBN was given by the microstructural changes.
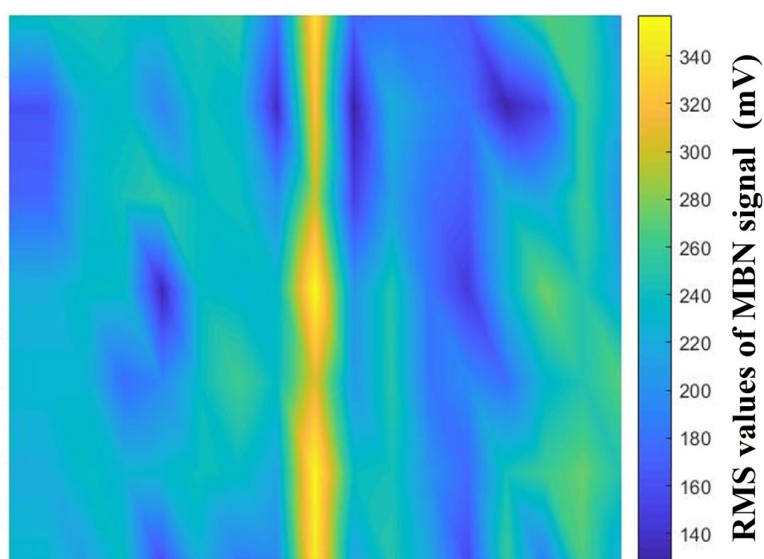

Figure 11. Heat map of the RMS values of the MBN signal obtained in the welded joint.
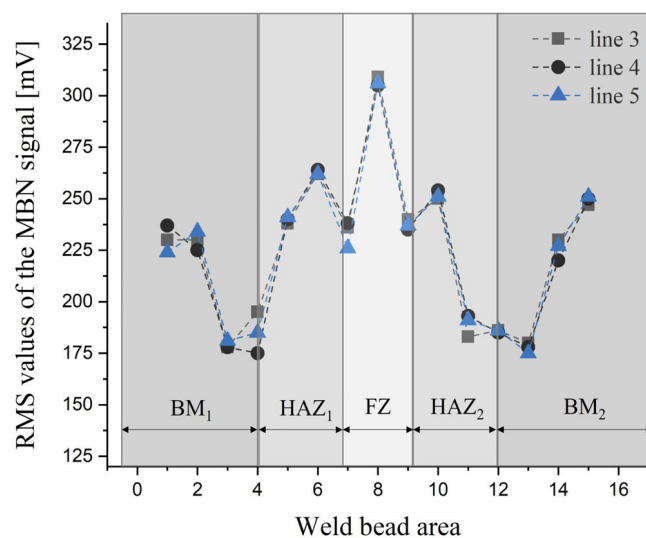
An Experimental Approach for Correlation of the Magnetic Barkhausen Noise to
Microstructural Changes and Residual Stress in Welding Joints

Liskevytch et al.

Figure 12. RMS values of MBN signal measured at the lines 3, 4 and 5.

The subsequent drop in the MBN signal to its minimum values in the BM_1 and BM_2 regions and its stabilization at the edges of the specimen accurately follows the transition from tensile to compressive residual stress measured values and their stabilization (Figure 10). A similar behavior of both the RMS values of the MBN and XRD-measured stresses was previously observed in joints produced with different welding processes by Vourna et al. [23], as demonstrated in Figure 2a, leading to the conclusion that in BM area the only influence on the MBN is given by the residual stress redistribution, all the more so BM do not suffer from microstructural and hardness changes by definition.

Overall, the experimental results of this study demonstrate that MBN is a sensitive tool for both microstructural and stress change analysis, including grain growth and refinement, and residual tensile and compressive magnitudes contribution. Demonstrated relationships might also alert users to an undesirable approximation of tensile stresses in the fusion area of the welded component to the material's yield strength when a 30-35% increase in the RMS values of the MBN is recorded (34% increase was reported in this study together with tensile stress reaching 79% of the material yield strength). This could potentially lead to distortions, cracks, and even catastrophic failures depending on the type of service applied (e.g., cyclic loading).

4. Conclusions

In the present study, a correlation between the MBN signal and microstructural changes due to the welding procedure, as well as induced residual stresses, was successfully established. Thus, for the magnetization parameters employed, the highest RMS values of the MBN were obtained in the fusion zone of the weld bead, where the highest values of Vickers hardness and tensile residual stresses were also measured. The lowest MBN values were observed in the base metal, where the lowest hardness values and compressive residual stresses were observed as well. However, contribution of these properties to the investigated signal differed in different areas of the welded joint. In the fusion zone, the influence of tensile residual stress was reported to be more notable, thereby increasing the MBN signal. In the heat affected zone, where stress magnitudes tended to be lower, the predominance of microstructure changes was observed together with a slight increase in the MBN values associated with grain growth and its subsequent refinement. Therefore, once again, the MBN technique proved to be an effective non-destructive tool for characterizing of welded structures, both for macro and microstructural changes, as well as for analyzing the distribution of residual stresses in different weld bead areas.

Authors' contributions

OL: writing – original draft, conceptualization, methodology, formal analysis. APFF: experimental results, formal analysis. EMA: experimental results. GFF: experimental results. RLMO: formal analysis, writing – review & editing. MCSM: conceptualization, fund raising.

An Experimental Approach for Correlation of the Magnetic Barkhausen Noise to
Microstructural Changes and Residual Stress in Welding Joints

Liskevytch et al.

Acknowledgements

References

[1] Scotti A. Five bars and one bar models for thermal stress generation in the FZ, HAZ and BM during arc welding. Soldagem e Inspeção. 2014;19(1):82-90. http://dx.doi.org/10.1590/S0104-92242014000100010.

[2] Colegrove PA, Ikeagu C, Thistlethwaite A, Williams S, Nagy T, Suder W, et al. Welding process impact on residual stress and distortion. Science and Technology of Welding and Joining. 2009;14(8):717-725. http://dx.doi.org/10.1179/136217109X406938.

[3] Vasantharaja P, Maduarimuthu V, Vasudevan M, Palanichamy P. Assessment of residual stresses and distortion in stainless steel weld joints. Materials and Manufacturing Processes. 2012;27(12):1376-1381. http://dx.doi.org/10.1080/10426914.2012.663135.

[4] Adak M, Guedes Soares C. Effects of different restraints on the weld-induced residual deformations and stresses in a steel plate. International Journal of Advanced Manufacturing Technology. 2014;71(1-4):699-710. http://dx.doi.org/10.1007/s00170-013-5521-9.

[5] Bhatti AA, Barsoum Z, Murakawa H, Barsoum I. Influence of thermomechanical material properties of different steel grades on welding residual stresses and angular distortion. Materials & Design. 2015;65:878-889. http://dx.doi.org/10.1016/j.matdes.2014.10.019.

[6] Gannon L, Liu Y, Pegg N, Smith M. Effect of welding sequence on residual stress and distortion in flat-bar stiffened plates. Marine Structures. 2010;23(3):385-404. http://dx.doi.org/10.1016/j.marstruc.2010.05.002.

[7] Perić M, Tonković Z, Rodić A, Surjak M, Garašić I, Boras I, et al. Numerical analysis and experimental investigation of welding residual stresses and distortions in a T-joint fillet weld. Materials & Design. 2014;53:1052-1063. http://dx.doi.org/10.1016/j.matdes.2013.08.011.

[8] Kudryavtsev Y, Kleiman J. Fatigue of welded elements: residual stresses and improvement treatments. In: Proceedings of the IIW International Conference on Welding & Materials; 2007 July 1-8; Dubrovnik, Croatia. Genoa: International Institute of Welding; 2007 [access 20 sep. 2023]. Available from: https://www.shotpeener.com/library/pdf/2008013.pdf

[9] Edwards L. Influence of residual stress redistribution on fatigue crack growth and damage tolerant design. Materials Science Forum. 2006;524-525:363-372. http://dx.doi.org/10.4028/www.scientific.net/MSF.524-525.363.

[10] Barsoum Z, Barsoum I. Residual stress effects on fatigue life of welded structures using LEFM. Engineering Failure Analysis. 2009;16(1):449-467. http://dx.doi.org/10.1016/j.engfailanal.2008.06.017.

[11] Xin H, Correia JAFO, Correia B, Veljkovic M, Berto F, Manuel L. Residual stress effects on fatigue life prediction using hardness measurements for butt-welded joints made of high strength steels. International Journal of Fatigue. 2021;147:106175. http://dx.doi.org/10.1016/j.ijfatigue.2021.106175.

[12] Hagenlocher C, Wagner J, Michel J, Weber R, Bachmann M, Karadogan C, et al. The influence of residual stresses on laser beam welding processes of aluminium sheets. In: Proceedings in 11th CIRP Conference on Photonic Technologies; 2020. Amsterdam: Elsevier; 2020. p. 713-717. http://dx.doi.org/10.1016/j.procir.2020.09.124.

[13] American Welding Society. AWS D1.1 structural welding code: steel. Miami: AWS; 2010.

[14] American Society of Mechanical Engineers. Boiler and pressure vessel code, section IX: welding, brazing and fusion qualifications. New York: ASME; 1999.

[15] Guo J, Fu H, Pan B, Kang R. Recent progress of residual stress measurement methods: a review. Chinese Journal of Aeronautics. 2021;34(2):54-78. http://dx.doi.org/10.1016/j.cja.2019.10.010.

[16] Jiles D. Introduction to magnetism and magnetic materials. New York: Chapman & Hall; 1994.

[17] Le Manh T, Benitez JAP, Hernandez JHE, Hallen JM. Barkhausen noise for non-destructive testing and materials characterization in low carbon steels. Duxford: Woodhead Publishing; 2020.

[18] Moorthy V, Shaw BA, Evans JT. Evaluation of tempering induced changes in the hardness profile of case-carburised EN36 steel using magnetic Barkhausen noise analysis. NDT & E International. 2003;36(1):43-49. http://dx.doi.org/10.1016/S0963-8695(02)00070-1.

[19] Desvaux M, Duquennoy J, Gualandri M, Ouaftouh MO, Ourak M. Evaluation of residual stress profiles using the Barkhausen noise effect to verify high performance aerospace bearings. Nondestructive Testing and Evaluation. 2005;20(1):9-24. http://dx.doi.org/10.1080/10589750412331315093.

[20] Kleber X, Vincent A. On the role of residual internal stresses and dislocations on Barkhausen noise in plastically deformed steel. NDT & E International. 2004;37(6):439-445. http://dx.doi.org/10.1016/j.ndteint.2003.11.008.

An Experimental Approach for Correlation of the Magnetic Barkhausen Noise to
Microstructural Changes and Residual Stress in Welding Joints

Liskevytch et al.

[21] Lasaosa K, Gurruchaga V, García Navas V, Martínez-de-Guereñu A. Characterization of in-depth stress state by magnetic Barkhausen noise on machined steel acquiring different frequency bands. Advanced Materials Research. 2014;996(373):373-379. http://dx.doi.org/10.4028/www.scientific.net/AMR.996.373.

[22] Mierczak P, Melikhov Y, Jiles DC. Determining residual stress depth profiles using the magnetic barkhausen effect. IEEE Transactions on Magnetics. 2014;50(10):1-5. http://dx.doi.org/10.1109/TMAG.2014.2329455.

[23] Vourna P, Ktena A, Tsakiridis PE, Hristoforou E. A novel approach of accurately evaluating residual stress and microstructure of welded electrical steels. NDT & E International. 2015;71:33-42. http://dx.doi.org/10.1016/j.ndteint.2014.09.011.

[24] Lasaosa A, Gurruchaga K, Arizti F, Martínez-de-Guerenu A. Quantitative estimation of nonmonotonic residual stress depth-profiles using an extended Kypris-Jiles model of the magnetic Barkhausen noise spectrum. Journal of Applied Physics. 2018;123(3):033904. http://dx.doi.org/10.1063/1.5002074.

[25] Yelbay I, Çam I, Gür CH. Non-destructive determination of residual stress state in steel weldments by Magnetic Barkhausen Noise technique. NDT & E International. 2010;43(1):29-33. http://dx.doi.org/10.1016/j.ndteint.2009.08.003.

[26] Landgraf FJG, Silveira JRF, Rodrigues D. Determining the effect of grain size and maximum induction upon coercive field of electrical steels. Journal of Magnetism and Magnetic Materials. 2011;323(18-19):2335-2339. http://dx.doi.org/10.1016/j.jmmm.2011.03.034.

[27] Sorsa A. Prediction of material properties based on non-destructive Barkhausen noise measurement. Oulu: University of Oulu; 2013.

[28] Serna-Giraldo CP, Padovese LR. Avaliação de soldagem de aço estrutural através do Ruído Magnético de Barkhausen. Soldagem e Inspeção. 2010;15(4):273-280. http://dx.doi.org/10.1590/S0104-92242010000400004.

[29] American Welding Society. Welding handbook. 8th ed. Vol. 1. Miami: AWS; 2001. Residual stresses and distortion.

[30] Ktena A, Hristoforou E, Gerhardt GJL, Missell FP, Landgraf FJG, Rodrigues DL Jr, et al. Barkhausen noise as a microstructure characterization tool. Physica B, Condensed Matter. 2014;435:109-112. http://dx.doi.org/10.1016/j.physb.2013.09.027.

[31] Steinzig M, Ponslet E. Residual stress measurements using the hole drilling method and laser speckle interferometry - Part II: analysis technique. Experimental Techniques. 2003;27(4):17-21. http://dx.doi.org/10.1111/j.1747-1567.2003.tb00117.x.

[32] Barile C, Casavola G, Pappalettera G, Pappalettere C. Analysis of the effects of process parameters in residual stress measurements on Titanium plates by HDM/ESPI. Measurement. 2014;48:220-227. http://dx.doi.org/10.1016/j.measurement.2013.11.014.

[33] Rahimi S, Violatos SRI. Comparison between surface and near - surface residual stress measurement techniques using a standard four - point - bend specimen. Experimental Mechanics. 2022;62(2):223-236. http://dx.doi.org/10.1007/s11340-021-00779-6.

[34] American Society for Testing and Materials. ASTM G39-99: standard practice for preparation and use of bent-beam stress-corrosion test specimens. West Conshohocken: ASTM; 2002.

[35] Liskevych O, Mesquita EA, Fracalossi G, Macêdo M. Estudo de aplicabilidade da técnica ESPI (Electronic Speckle Pattern Interferometry) combinada com o método do furo-cego para medição de tensões residuais em juntas soldadas. In: Anais do XI Congresso Nacional de Engenharia Mecânica (CONEM); 2022; Teresina, PI. Rio de Janeiro: ABCM; 2022. http://dx.doi.org/10.26678/ABCM.CONEM2022.CON22-0780.

[36] Stresstech Oy. Prism technical guide. 4th ed. Vol. 2. Jyvaskyla; 2016.